

---

# Learning Protein Representations via Complete 3D Graph Networks

---

**Limei Wang\***

Texas A&M University  
College Station, TX 77843  
limei@tamu.edu

**Haoran Liu\***

Texas A&M University  
College Station, TX 77843  
liuhr99@tamu.edu

**Yi Liu\*<sup>†</sup>**

Texas A&M University  
College Station, TX 77843  
yiliu@tamu.edu

**Jerry Kurtin**

Texas A&M University  
College Station, TX 77843  
jkurtin@tamu.edu

**Shuiwang Ji<sup>†</sup>**

Texas A&M University  
College Station, TX 77843  
sji@tamu.edu

## Abstract

We consider representation learning for proteins with 3D structures. We build 3D graphs based on protein structures and develop graph networks to learn their representations. Depending on the levels of details that we wish to capture, protein representations can be computed at different levels, *e.g.*, the amino acid, backbone, or all-atom levels. Importantly, there exist hierarchical relations among different levels. In this work, we propose to develop a novel hierarchical graph network, known as ProNet, to capture the relations. Our ProNet is very flexible and can be used to compute protein representations at different levels of granularity. We show that, given a base 3D graph network that is complete, our ProNet representations are also complete at all levels. To close the loop, we develop a complete and efficient 3D graph network to be used as a base model, making our ProNet complete. We conduct experiments on multiple downstream tasks. Results show that ProNet outperforms recent methods on most datasets. In addition, results indicate that different downstream tasks may require representations at different levels. Our code is available as part of the DIG library (<https://github.com/dive1ab/DIG>).

## 1 Introduction

Proteins consist of one or more amino acid chains and perform various functions by folding into 3D conformations. Learning representations from proteins with 3D structures is crucial for a wide range of tasks [7, 52, 61, 63, 15, 51, 40]. In machine learning, molecules and proteins are usually modeled as graphs [30, 36, 13, 40, 27, 17, 16]. With the advances of deep learning, 3D graph neural networks (GNNs) have been developed to learn from 3D graph data [30, 27, 62, 34]. In this work, we build 3D graphs based on protein structures and develop 3D GNNs to learn protein representations.

Depending on the levels of granularity we wish to capture, we construct protein graphs at different levels, including the amino acid, backbone, and all-atom levels, as shown in Fig. 1. Specifically, each node in constructed graphs represents an amino acid, and each amino acid possesses internal structures at different levels. Importantly, there exist hierarchical relations among different levels. Existing methods for protein representation learning either ignore hierarchical relations within proteins [26, 33, 20, 64], or suffer from excessive computational complexity [25, 21]. In this work,

---

\*Equal contribution

<sup>†</sup>Equal senior contribution

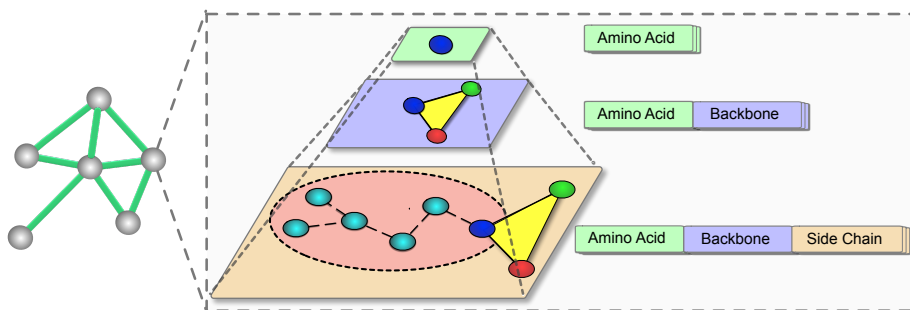


Figure 1: Illustration of hierarchical representations for protein structures. Each node in the left graph denotes an amino acid, whose internal hierarchical representation is shown in the zoom-in view. From top to bottom, three hierarchical levels are namely the amino acid level, the backbone level, and the all-atom level, respectively. The actual graphs are in 3D, and this illustration uses 2D for simplicity.

we propose a novel hierarchical graph network, known as ProNet, to learn protein representations at different levels. Our ProNet effectively captures the hierarchical relations naturally present in proteins. To fully capture 3D information with reasonable computational cost, we further develop a complete and efficient 3D graph network as the base model. Building on such based model, we show our ProNet achieves complete representations for all levels efficiently.

By constructing representations at different levels, our ProNet effectively integrates the inherent hierarchical relations of proteins, resulting in a more rational protein learning scheme. Building on a novel hierarchical fashion, our method can achieve great efficiency, even at the most complex all-atom level. In addition, completeness at all levels enable models to generate informative and discriminative representations. Practically, ProNet possesses great flexibility for different data and downstream tasks. Users can easily choose the level of granularity at which the model should operate based on their data and tasks. We conduct experiments on multiple downstream tasks, including protein fold and function prediction, protein-ligand binding affinity prediction, and protein-protein interaction prediction. Results show that ProNet outperforms recent methods on most datasets. We also show that different data and tasks may require representations at different levels.

## 2 Hierarchical Representations of Protein Structures

### 2.1 Background

Proteins are highly complex macromolecules consisting of one or more chains of amino acids. Each chain may contain up to hundreds or even thousands of amino acids. Despite the vast variety of proteins in nature, proteins in living organisms are made up of 20 different types of amino acids. An amino acid consists of an amino ( $-\text{NH}_2$ ) group, a carboxylic acid ( $-\text{COOH}$ ) group, and an organic R group (also known as the side chain) that is unique to each amino acid. The functional groups are all attached to a central carbon atom, known as the alpha carbon ( $C_\alpha$ ) [39]. The alpha carbons in the peptide chains, together with the corresponding amino group and carboxylic group, form the backbones of proteins. As shown in Fig. 1, for a protein, we represent each amino acid at three levels to capture different levels of the structure. Note that protein structures are traditionally organized into primary, secondary, tertiary, and quaternary levels, and our categorization of levels is different.

### 2.2 Notations & Definitions

**3D Protein Graphs.** Given a protein structure, we construct a 3D protein graph  $G = (\mathcal{V}, \mathcal{E}, \mathcal{R})$ . Here,  $\mathcal{V} = \{\mathbf{v}_i\}_{i=1, \dots, n}$  is the set of node features, where each  $\mathbf{v}_i \in \mathbb{R}^{d_v}$  denotes the feature vector for node  $i$ . Importantly, we treat each amino acid in the protein as a node in this study.  $\mathcal{E} = \{\mathbf{e}_{ij}\}_{i,j=1, \dots, n}$  is the set of edges, where  $\mathbf{e}_{ij} \in \mathbb{R}^{d_e}$  denotes the edge feature vector for edge  $ij$ . Particularly,  $\mathcal{R} = \{R_i\}_{i=1, \dots, n}$  is the set of position matrices, where  $R_i \in \mathbb{R}^{k_i \times 3}$  denotes the position matrix for amino acid  $i$ . As shown in Fig. 1, an amino acid possesses a detailed inner structure at each hierarchical level. To further represent such inner structures, we use  $k_i$  to denote the number of units for amino acid  $i$  at each hierarchical level. Based on Sec. 2.1, we set  $k_i = 1$  for the amino acid level,  $k_i = 3$  for the backbone level, and  $k_i$  as the total number of atoms in amino acid  $i$  for the all-atom level. As the structure for a specific unit is fixed, we follow commonly-adopted settings and use an atom to represent the corresponding unit [27]. For example, as introduced in Sec. 2.1, a backbone

plane consists of three units including an  $\text{-NH}_2$  group, the center  $C_\alpha$ , and a  $\text{-COOH}$  group. We simply use  $N$ ,  $C_\alpha$ , and  $C$  to represent them, respectively. Obviously, each 3-dimensional row vector in  $R_i$  contains the Cartesian coordinates for the corresponding atom. Note that the rows in  $R_i$  are given in a fixed atom order for each amino acid  $i$ . For example, for the amino acid alanine at the all-atom level, the atom order in the position matrix is  $N$ ,  $C_\alpha$ ,  $C$ ,  $O$ , and  $C_\beta$ . By doing this,  $R_i$  contains both the atom type and 3D coordinates for each atom in an amino acid  $i$ . Hence,  $R_i$  contains all the necessary information to determine the structure of an amino acid at any level.

**Geometric Representation.** To fulfill  $\text{SE}(3)$  invariance of a given 3D protein graph, we further define a geometric representation function  $\mathcal{F}$ , which maps the 3D graph  $G$  to a geometric representation (GR)  $\mathcal{F}(G)$ . A GR is a set of tuples, each of which contains different geometric information. There are several  $\text{SE}(3)$  invariant graph learning methods [47, 30, 36, 31] in literature, and these methods consider different GRs. For example, SchNet [47] computes the distance for each edge. Hence, the length of the GR set is the number of edges, and each tuple contains one distance; SphereNet [36] computes a distance, an angle, and a torsion angle for each triplet of nodes. Hence, the set length is the number of triplets, and each tuple contains three geometries.

**ProNet.** In this work, we propose to develop a novel hierarchical graph network, known as ProNet, for protein graph learning. We first define the message passing scheme [18] for our ProNet as

$$\mathbf{v}'_i = \text{UPDATE} \left( \mathbf{v}_i, \sum_{j \in \mathcal{N}_i} \text{MESSAGE}(\mathbf{v}_j, \mathbf{e}_{ji}, \mathcal{F}(G)) \right), \quad (1)$$

where  $\mathcal{N}_i$  denotes the set of node  $i$ 's neighbors, and UPDATE and MESSAGE functions are usually implemented by neural networks or simpler mathematical operations. In particular, we consider the GR  $\mathcal{F}(G)$  to capture geometric information of input 3D protein graphs. Importantly,  $\mathcal{F}(G)$  is varying across different hierarchical levels. For levels from top to bottom in Fig. 1, we specify the designed GR as  $\mathcal{F}(G)_{\text{base}}$ ,  $\mathcal{F}(G)_{\text{bb}}$ , and  $\mathcal{F}(G)_{\text{all}}$ , respectively. The final protein representation  $\mathbf{g}$  is obtained as

$$\mathbf{g} = \text{READOUT}(\{\mathbf{v}_i^L\}_{i=1, \dots, n}). \quad (2)$$

Here,  $\mathbf{v}_i^L$  indicates the feature vector of node  $i$  at the last layer. A READOUT function can be either mathematical functions such as summation or mean, or mathematical functions followed by fully-connected layers. Apparently, through the proposed GR  $\mathcal{F}(G)$ , ProNet is able to compute protein representations at different hierarchical levels.

**A Novel and Different Hierarchical Fashion.** Our ProNet presents a novel hierarchical learning fashion considering domain knowledge of proteins for effective and efficient learning. Specifically, ProNet treats each amino acid as a node and learns from different levels of inner structures within amino acids. Essentially, ProNet captures hierarchical relations inside an amino acid from the geometry perspective. Our hierarchical fashion is different from the mainstream hierarchical pipeline, which first treats each atom as a node and then treats inner structures at each level as subgraphs, finally employing 3D GNNs at each level to learn from these subgraphs and obtain representations as node features for the next level. Overall, the merits of our proposed hierarchical fashion are threefold. Firstly, the number of amino acids is much smaller than that of atoms in proteins. Hence, by treating each amino acid as a node, our fashion generates much smaller 3D graphs. Secondly, our method needs one 3D graph model with different GRs for each level based on domain knowledge of proteins. However, the mainstream fashion simply treats inner structures at each hierarchical level as 3D graphs, then needs one 3D graph model for each hierarchical level. Thus, the number of the used models is equal to that of the levels. Finally, our fashion has great flexibility to generate representations at all levels, while the mainstream method can only operate at the all-atom level. We demonstrate in Sec. 6.5 that the hierarchical fashion used in ProNet achieves slightly better performance and dramatically improved efficiency compared with the mainstream method.

### 2.3 Amino Acid Level

As proteins consist of amino acids, we naturally treat each amino acid as a node in protein graphs. Particularly, the coordinates for the center  $C_\alpha$  are used as the position information of the node. This renders the most coarse-grained representation of each amino acid and the protein as shown in Fig. 1. Then we use a cutoff radius to define edges between nodes. Specifically, if the distance between two nodes is less than a predefined radius, there is an edge between these two nodes. Eventually,

we construct a 3D graph  $G = \{\mathcal{V}, \mathcal{E}, \mathcal{R}\}$  for each protein, as defined in Sec. 2.2. For each node  $i$ , we use the one-hot embedding of the amino acid type as the initial node feature  $\mathbf{v}_i$ . A protein chain is essentially a sequence of amino acids, and such sequential information is shown to be crucial to determine protein functions. Hence, we follow existing studies [24, 64] and integrate the sequential information in edge features. Specifically, for each edge  $ij$  that is from node  $i$  to node  $j$ , the edge feature includes an embedding of the sequential distance  $j - i$ . The shape of the position matrix  $R_i$  of a node  $i$  is  $1 \times 3$  since we only consider the position of the center  $C_\alpha$  at this level. After constructing 3D protein graphs, we design an appropriate GR  $\mathcal{F}(G)_{\text{base}}$  for our ProNet to encode 3D information at this level. Existing learning methods for 3D graphs either integrate partial 3D information or induce high computing complexity. For the purpose of accurate and efficient protein learning, we carefully design  $\mathcal{F}(G)_{\text{base}}$ , which is introduced in Sec. 4.

## 2.4 Backbone Level

Building on the proposed amino acid level representation, we further introduce the backbone structure for each amino acid to derive finer-grained protein representations. To this end, we propose the backbone level representation for our ProNet, as illustrated in Fig. 1. The position matrix  $R_i \in \mathbb{R}^{3 \times 3}$  for each node  $i$  contains three row vectors  $\mathbf{r}_i^N, \mathbf{r}_i^{C_\alpha}, \mathbf{r}_i^C$ , corresponding to the coordinates of atoms  $N_i, C_{\alpha_i}, C_i$  in the  $i$ -th amino acid, respectively. As the bond lengths and angles in a backbone triangle are fixed, we treat the backbone structure of an amino acid as a rigid triangle.

Apparently, as we treat amino acid backbones as rigid triangles, the remaining degree of freedom for geometric transformation is the rotation between two backbone planes. We propose to compute Euler angles to describe such rotation. Specifically, we compute three Euler angles  $\tau^1, \tau^2$ , and  $\tau^3$  between any two backbone coordinate systems. Firstly, we define a local coordinate system for the backbone of any amino acid  $i$  with three orthogonal vectors  $\mathbf{x}_i, \mathbf{y}_i, \mathbf{z}_i$ . As shown in Fig. 2(a), we compute the vectors as  $\mathbf{y}_i = \mathbf{r}_i^N - \mathbf{r}_i^{C_\alpha}$ ,  $\mathbf{t}_i = \mathbf{r}_i^C - \mathbf{r}_i^{C_\alpha}$ ,  $\mathbf{z}_i = \mathbf{t}_i \times \mathbf{y}_i$ , and  $\mathbf{x}_i = \mathbf{y}_i \times \mathbf{z}_i$ . We then define the Euler angles between the backbone local coordinate systems of two amino acids  $i$  and  $j$ . As show in Fig. 2(b), the intersection of two local systems is identified by the normal vector  $\mathbf{n} = \mathbf{z}_i \times \mathbf{z}_j$ . Based on this, the Euler angle  $\tau_{ij}^1$  indicates the signed angle between  $\mathbf{n}$  and  $\mathbf{x}_i$ ,  $\tau_{ij}^2$  is the angle between  $\mathbf{z}_i$  and  $\mathbf{z}_j$ , and  $\tau_{ij}^3$  is the angle from  $\mathbf{n}$  to  $\mathbf{x}_j$ . By considering these three Euler angles, the orientation between any two backbone planes can be fixed. Thus, we formally write the GR for our ProNet at this level as  $\mathcal{F}(G)_{\text{bb}} = \mathcal{F}(G)_{\text{base}} \cup \{(\tau_{ji}^1, \tau_{ji}^2, \tau_{ji}^3)\}_{i=1, \dots, n, j \in \mathcal{N}_i}$ .

Note that most existing approaches directly integrate backbone structural information into amino acid features. These methods firstly compute three backbone torsion angles  $\omega^1, \omega^2$ , and  $\omega^3$  [24, 25, 15, 33] for each amino acid as shown in Fig. 2(c). Specifically, for the  $i$ -th amino acid,  $\omega_i^1, \omega_i^2$ , and  $\omega_i^3$  are the bond rotation angles for the bonds connecting  $N_i$  and  $C_{\alpha_i}, C_{\alpha_i}$  and  $C_i$ , and  $C_i$  and  $N_{i+1}$ , respectively. Then they compute sin and cos values for the three torsion angles as part of the node features of amino acid  $i$ . For any two amino acids  $i$  and  $j$ , if we safely assume  $j > i$ , the relative rotation of these two backbone triangles is determined by all the amino acids between  $i$  and  $j$  along the protein chain. Thus, the relative rotation is determined by all the  $(j - i + 1) \times 3$  bond rotation angles  $\{\omega_k^1, \omega_k^2, \omega_k^3\}_{k=i, \dots, j}$ , as shown in Fig. 2(c). However, our proposed backbone level method can determine the relative rotation for any two amino acids  $i$  and  $j$  by computing only three Euler angles  $\tau_{ji}^1, \tau_{ji}^2$ , and  $\tau_{ji}^3$ , regardless of the sequential distance  $j - i$  along the protein chain. Hence, our method can largely improve the efficiency for representation learning at this level.

## 2.5 All-Atom Level

To obtain the most fine-grained representations of proteins, we consider all atoms in each amino acid. Hence, different from the constructed 3D graphs for the above two levels, the position matrix  $R_i$  contains the positions of all atoms in amino acid  $i$ . As introduced in Sec. 2.1, an amino acid consists of a backbone and a side chain. Building on our backbone level representation, we further incorporate side chain information, leading to the all-atom level representation for our ProNet as in Fig. 1.

As all bond lengths and bond angles in each amino acid are fully rigid, the degree of freedom we need to consider is torsion angles in side chains [27]. There are at most five torsion angles for any amino acid. For example, as shown in Fig. 3 in Appendix A, the alanine has zero side chain torsion angle, the cysteine has only one, and the leucine has two. Note that only the amino acid arginine has five side chain torsion angles, and the fifth angle is close to 0. Therefore, we only consider the first four torsion

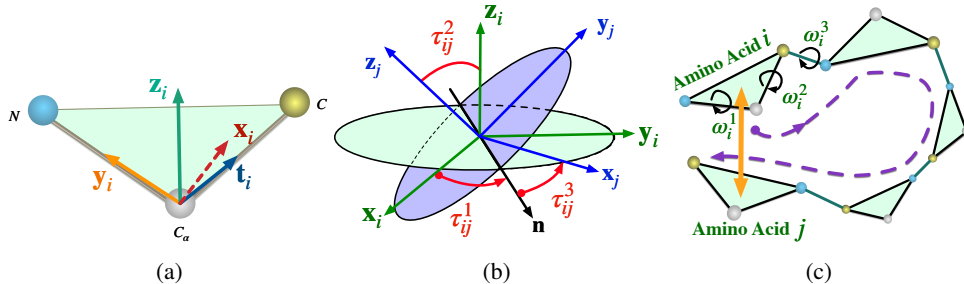


Figure 2: Illustrations of our proposed backbone-level representation. (a) Construction of the backbone coordinate system for amino acid  $i$ . (b) Computing of the three Euler angles between the backbone coordinate systems for two amino acids  $i$  and  $j$ . (c) Illustrations of determining the relative rotation between amino acids  $i$  and  $j$  for existing methods and our proposed method. The purple dashed line indicates how existing methods determine the relative rotation between  $i$  and  $j$  by computing all backbone torsion angles along the chain. The yellow arrow shows how our method determines the relative rotation between amino acids  $i$  and  $j$  using only three Euler angles.

angles in side chains for efficiency, denoted as  $\chi^1, \chi^2, \chi^3, \chi^4$ . We list the atoms used to compute side chain torsion angles for each amino acid in Table 5 in Appendix A. With such side chain torsion angles, we can determine the side chain structure for each amino acid. Based on the backbone level representation, the GR for our ProNet at this level is  $\mathcal{F}(G)_{\text{all}} = \mathcal{F}(G)_{\text{bb}} \cup \{(\chi_i^1, \chi_i^2, \chi_i^3, \chi_i^4)\}_{i=1, \dots, n}$ .

There exist several studies also considering all-atom information of proteins [21, 25]. IEConv [21] employs the mainstream hierarchical fashion as introduced in Sec. 2.2. At the first level, It treats each atom as a node in constructed 3D protein graphs. Then it proposes several pooling layers to obtain representations for following hierarchical levels. For each hierarchical level, IEConv needs one 3D model with several intrinsic-extrinsic convolution layers for message passing. By treating each atom as a node and employing several 3D models, IEConv induces excessive computing cost. The vector-gated GVP-GNN [25] also treats each atom as a node in the graph and uses equivariant GNNs to update node features. However, the important hierarchical information is neglected in GVP-GNN. Our proposed method effectively incorporates all-atom information with preserving hierarchical relations naturally present in proteins. In addition, by treating one amino acid as a node and integrating side chain torsion angles as node features, our method has much fewer nodes in constructed graphs, resulting in a much more efficient learning scheme.

### 3 Completeness Analysis

In this section, we study the completeness of the geometric representation for each hierarchical level of our ProNet introduced in Sec. 2. Complete GRs capture all details of 3D protein structures and thus enable our ProNet to generate distinct representations for different 3D protein graphs. We first provide the formal definition of completeness for 3D protein graphs as below.

**Definition 1** (Completeness). *For two protein graphs  $G^1 = (\mathcal{V}, \mathcal{E}, \mathcal{R}^1)$  and  $G^2 = (\mathcal{V}, \mathcal{E}, \mathcal{R}^2)$ , where  $\mathcal{R}^1 = \{R_i^1\}_{i=1, \dots, n}$  and  $\mathcal{R}^2 = \{R_i^2\}_{i=1, \dots, n}$ , respectively, a geometric representation  $\mathcal{F}(G)$  is considered complete if*

$$\mathcal{F}(G^1) = \mathcal{F}(G^2) \iff \exists T \in SE(3), \text{ for } i = 1, \dots, n, \mathcal{R}_i^1 = T(\mathcal{R}_i^2). \quad (3)$$

To demonstrate whether a GR  $\mathcal{F}(G)$  is complete, we need to prove in both aspects as below. We first need to show Eq. 3 holds from right to left, which is obvious in principle. This is because our proposed GR generates relative information such as distance, it is then naturally  $SE(3)$  invariant. In addition, the only difference between  $G^1$  and  $G^2$  lies in  $R^1$  and  $R^2$ . Hence, for each  $i$ , if  $\mathcal{R}_i^1$  and  $\mathcal{R}_i^2$  are in the same  $SE(3)$  group,  $\mathcal{F}(G^1) = \mathcal{F}(G^2)$  naturally holds. Secondly, we need to prove Eq. 3 holds from left to right. Essentially, to show a GR  $\mathcal{F}(G)$  is complete, we need to prove that a 3D structure can be uniquely determined by this  $\mathcal{F}(G)$ . In the research area of 3D graph learning, there exist several 3D graph models that are either approximately complete or complete [36, 31]. In the rest of this section, we assume we have a complete base  $\mathcal{F}(G)_{\text{base}}$  for regular 3D graphs, then further prove that  $\mathcal{F}(G)_{\text{bb}}$  and  $\mathcal{F}(G)_{\text{all}}$  are both complete.

### 3.1 Completeness of the Amino Acid Level

Given a protein, the constructed 3D protein graph at the amino acid level is a regular 3D graph [36]. By employing a base model with complete geometric representation  $\mathcal{F}(G)_{\text{base}}$ , the graph structure can be uniquely determined. Thus, completeness is naturally achieved at this level. More details about the complete base models are provided in Sec. 4.

### 3.2 Completeness of the Backbone Level

Given a complete  $\mathcal{F}(G)_{\text{base}}$  and based upon the proposed Euler angles  $\tau^1, \tau^2$ , and  $\tau^3$  in Sec. 2.4, the proposed GR  $\mathcal{F}(G)_{\text{bb}}$  for the backbone level is complete, as stated in the following proposition.

**Proposition 1.** *For a connected 3D protein graph  $G = (\mathcal{V}, \mathcal{E}, \mathcal{R})$  of the backbone level in which  $\mathcal{R} = \{R_i\}_{i=1, \dots, n}$  and  $R_i \in \mathbb{R}^{3 \times 3}$ , given a complete geometric representation  $\mathcal{F}(G)_{\text{base}}$ , the geometric representation  $\mathcal{F}(G)_{\text{bb}} = \mathcal{F}(G)_{\text{base}} \cup \{(\tau_{j_i}^1, \tau_{j_i}^2, \tau_{j_i}^3)\}_{i=1, \dots, n, j \in \mathcal{N}_i}$  is **complete**.*

We provide rigorous proof for Prop. 1 in Appendix B.1. Intuitively, a complete GR at the backbone level can capture all 3D information of the backbone structure of a protein. As protein backbones largely determine protein functions, capturing fine details of them can benefit various tasks. Specifically, a protein backbone is connected by covalent bonds and hydrogen bonds. Patterns of hydrogen bonds determine the secondary structure of the protein [38, 41]. Therefore, our complete representations of backbone structures enable models to learn how a protein sequence folds into the secondary structure and further forms into current conformation, eventually determining protein functions.

### 3.3 Completeness of the All-Atom Level

As introduced in Sec. 2.5, the GR for the all-atom level  $\mathcal{F}(G)_{\text{all}}$  considers four side chain torsion angles  $\chi_i^1, \chi_i^2, \chi_i^3, \chi_i^4$ . Given a complete backbone representation  $\mathcal{F}(G)_{\text{bb}}$ ,  $\mathcal{F}(G)_{\text{all}}$  is complete as claimed in the following proposition.

**Proposition 2.** *For a connected 3D protein graph  $G = (\mathcal{V}, \mathcal{E}, \mathcal{R})$  of the all-atom level, given a complete geometric representation  $\mathcal{F}(G)_{\text{bb}}$ , the geometric representation  $\mathcal{F}(G)_{\text{all}} = \mathcal{F}(G)_{\text{bb}} \cup \{(\chi_i^1, \chi_i^2, \chi_i^3, \chi_i^4)\}_{i=1, \dots, n}$  is **complete**.*

The proof for Prop. 2 is provided in Appendix B.2. With the complete GR at the all-atom level, our method can fully capture 3D information of all atoms in a protein. Therefore, our method can distinguish any two distinct protein structures in nature. Especially, our all-atom method can capture side chain structures compared with the backbone level method. Side chains are important for proteins. The only difference among the 20 types of amino acids lies in distinct side chains [50]. Especially, the tertiary and quaternary structures of a protein are determined by interactions between side chains and environment [44]. In addition, interactions between side chains also play a crucial role in protein-protein and protein-ligand interactions [54, 4]. Overall, the all-atom method can capture more information for both inter- and intra-protein interactions, largely affecting protein functions.

## 4 Complete and Efficient Base Models

As introduced in Sec. 3.1, protein graphs at the amino acid level are regular 3D graphs. With a complete base model, we can achieve completeness at the amino acid level. There exist several 3D graph learning models [47, 30, 36, 31], among which SphereNet [36] is shown to be approximately complete. However, SphereNet is still not rigorously complete and not efficient enough for processing large protein graphs. To this end, we propose a complete and efficient model based on SphereNet [36]. Specifically, we first propose our complete GR  $\mathcal{F}(G)_{\text{base}}$ . Besides, our proposed message passing scheme also reduces the complexity by orders of magnitude compared with SphereNet. Finally, we slightly change the network architecture of SphereNet as the architecture of our ProNet in this study.

Similar to SphereNet, our  $\mathcal{F}(G)_{\text{base}}$  can also be built on the spherical coordinate system. However, we propose a novel strategy to build the local coordinate systems. Specifically, for a protein graph at the amino acid level, we define a local coordinate system for each center node  $i$  based on the positions of nodes  $i, i-1$ , and  $i+1$ . Their positions are denoted as  $\mathbf{r}_i, \mathbf{r}_{i-1}$ , and  $\mathbf{r}_{i+1}$ , respectively. Here  $i-1$  and  $i+1$  are the two adjacent amino acids of node  $i$  in the amino acid sequence. We set the direction of  $\mathbf{r}_{i-1} - \mathbf{r}_i$  as  $z$ -axis, and the direction of  $(\mathbf{r}_{i-1} - \mathbf{r}_i) \times (\mathbf{r}_{i+1} - \mathbf{r}_i)$  as  $y$ -axis. Here  $\times$  operation

denotes cross product between two vectors. Then  $x$ -axis is simply the cross product between  $y$ -axis and  $z$ -axis. With the built local coordinate system, the relative position of node  $j \in \mathcal{N}_i$  to node  $i$  can be specified by the 3-tuple  $(d, \theta, \phi)$  as in SphereNet. However, if we rotate the edge  $ji$ ,  $i$ 's local neighborhood keeps fixed, but the whole structure changes. Apparently, the edge rotation angle  $\tau$  is the only remaining degree of freedom to achieve completeness on the protein graph. Hence, we further include  $\tau_{ji}$ , which is computed based on the positions of nodes  $i, j, i-1, i+1, j-1$ , and  $j+1$ . Finally, for each neighboring node  $j$  of a center node  $i$ , we derive a complete geometric representation  $\mathcal{F}(G)_{\text{base}} = \{(d_{ji}, \theta_{ji}, \phi_{ji}, \tau_{ji})\}_{i=1, \dots, n, j \in \mathcal{N}_i}$ . Detailed computing of the used four geometries is provided in Appendix C. Compared with SphereNet, our GR is able to guarantee completeness of the whole graph. In addition, SphereNet operates in 2-hop neighborhood, resulting in a complexity of  $O(nk^2)$  [36]. Here  $n$  is the number of nodes in the graph, and  $k$  is the average degree. Our message passing scheme computes the 4-tuple  $(d, \theta, \phi, \tau)$  within 1-hop neighborhood, significantly reducing the complexity to  $O(nk)$ . Based on the proposed complete  $\mathcal{F}(G)_{\text{base}}$  and message passing scheme, we design complete and efficient base models for protein learning. Overall, our base models are adapted from SphereNet considering our complete  $\mathcal{F}(G)_{\text{base}}$  and efficient message passing scheme in Eq. 1. Detailed description of the network architecture of ProNet is in Appendix C.

## 5 Related Work

**Protein representation learning.** Learning protein representations is essential to a variety of tasks in protein engineering [7, 52, 61, 63, 15, 51, 40, 35]. Existing methods for protein learning consider different kinds of protein information, including amino acid sequences [43, 3, 46, 11, 6], protein surfaces [14, 53, 8, 49], and protein 3D structures [13, 19, 2, 21, 20, 26, 25, 33, 64]. Due to recent advances in protein structure prediction [48, 27, 57, 1], structures of many proteins are becoming available with high accuracy. In addition, protein structures are crucial to determining protein functions. In this work, we focus on representation learning for proteins with 3D structures. Earlier studies formulate proteins as 3D grid-like data and employ 3D CNNs for learning [10, 56]. However, grid-like protein data is extremely sparse, leading to expensive learning cost and unsatisfactory performance. Hence, recent studies use 3D GNNs to process protein data modeled as 3D protein graphs [21, 20, 26, 24, 64, 33]. Based on the analysis in Sec. 2, previous methods on 3D protein graphs can be categorized into three levels, including amino acid level, backbone level, and all-atom level, as listed in detail in Appendix D. For example, GearNet [64] treats an amino acid as a node in protein graphs and uses amino acid types as node features, thus it is categorized as an amino acid level method. GVP-GNN [26] represents protein backbone structures with backbone dihedral angles computed from backbone atoms. Thus it is a backbone level method. IEConv [21] treats each atom as a node in protein graphs, therefore, it is an all-atom level method.

### Differences with our methods.

Existing methods on 3D protein graphs either neglect the important hierarchical relations naturally present in proteins, or induce excessive computing complexity. For example, to capture geometric information of all atoms, the vector-gated GVP-GNN [25] treats each atom as a node in graphs and uses equivariant GNNs to update node features. Even though such atom-level learning method can be applied to a wide range of tasks as shown in Jing et al. [25], it fails to consider the important hierarchical information of proteins. As a result, the model can hardly infer inherent inner structures such as obtain backbones, side chains, or amino acids. In addition, as the number of atoms is much larger than that of amino acids in proteins, treating each atom as a node will generate extremely large 3D graphs. IEConv [21] employs the mainstream hierarchical fashion as introduced in Sec. 2.2. It also treats each atom as a node in graphs and uses hierarchical pooling layers to capture hierarchical information. There needs to be one 3D graph model for each hierarchical level and a 3D model usually consists of several message passing layers. Overall, IEConv introduces excessive computing complexity.

## 6 Experiments

We evaluate our ProNet on various protein tasks, including protein fold and reaction prediction, protein-ligand binding affinity prediction, and protein-protein interaction prediction. We also conduct ablation study on the design of our all-atom method. The implementation of our methods is based on the PyTorch [45] and Pytorch Geometric [12], and all models are trained with the Adam optimizer [28].

Detailed experimental setup and optimal hyperparameters are provided in Appendix E. Code is in the DIG library [34] and available at <https://github.com/divelab/DIG>.

## 6.1 Fold Classification

Protein fold classification [22, 32] is crucial to capture protein structure-function relations and protein evolution. Following the dataset and experimental settings in Hou et al. [22] and Hermosilla et al. [21], we evaluate the performance of our methods on the fold classification task. A detailed description of the data is provided in Appendix F. There are three test sets, including Fold, Superfamily, and Family. We report the accuracies on the three test sets and the average of the three accuracy values in Table 1. The results for baseline methods are taken from original papers [21, 49, 64, 33].

Table 1 shows that our methods achieve the best results on two of the three test sets and the best average value. For Superfamily and Family, our methods outperform all of the baseline methods and achieve similar performance as GearNet-Edge-IEConv. But GearNet-Edge-IEConv uses edge message passing scheme, which is more computational expensive than the node message passing scheme in our method, as discussed in Sec. 4 and Liu et al. [36]. For Fold, the most difficult one among the three test sets, all of our methods on three levels can significantly outperform baseline methods, and our ProNet-backbone improves the accuracy from 48.3% to 52.7%. Our methods also improve the average value from 72.7% to 74.1% and set the new state of the art.

## 6.2 Reaction Classification

Enzymes are proteins that act as biological catalysts. They can be classified with enzyme commission (EC) numbers which groups enzymes based on the reactions they catalyze [60, 42]. We follow the dataset and experiment settings in Hermosilla et al. [21] to evaluate our methods on this task. In total, this dataset contains 37,428 proteins from 384 EC numbers [5, 9]. Comparison results are summarized in Table 1, where the results for baseline methods are taken from original papers [21, 20, 33, 64]. Our methods achieve better or comparable results compared with previous methods. Note that IEConv methods [21, 20] are complicated and have larger numbers of parameters.

Table 1: Accuracy (%) on fold and reaction classification. The top two results are highlighted as **1st** and 2nd.

Method	React	Fold			
		Fold	Sup.	Fam.	Avg.
GCN [29]	67.3	16.8	21.3	82.8	40.3
DeepSF [22]	70.9	17.0	31.0	77.0	41.7
GVP-GNN [26]	65.5	16.0	22.5	83.8	40.8
IEConv [21]	<b>87.2</b>	45.0	69.7	98.9	71.2
New IEConv [20]	<b>87.2</b>	47.6	<u>70.2</u>	99.2	72.3
HoloProt [49]	78.9	–	–	–	–
DWNN [33]	76.7	31.8	37.8	84.8	51.5
GearNet [64]	79.4	28.4	42.6	95.3	55.4
GearNet-IEConv [64]	83.7	42.3	64.1	99.1	68.5
GearNet-Edge [64]	86.6	44.0	66.7	99.1	69.9
GearNet-Edge-IEConv [64]	85.3	48.3	<b>70.3</b>	<b>99.5</b>	72.7
ProNet-Amino Acid	86.0	51.5	69.9	99.0	<u>73.5</u>
ProNet-Backbone	86.4	<b>52.7</b>	<b>70.3</b>	<u>99.3</u>	<b>74.1</b>
ProNet-All-Atom	85.6	<u>52.1</u>	69.0	99.0	73.4

Specifically, the numbers of parameters for IEConv methods are about 10M and 20M, while that of our methods are less than 2M. Notably, our ProNet-backbone performs best among three levels. This may indicate that our backbone level can capture more details from folding structures of proteins and thus has better predictions for protein functions.

## 6.3 Ligand Binding Affinity

Computational prediction of protein-ligand binding affinity (LBA) is essential for many downstream tasks in drug discovery as it mitigates the cost of wet-lab experiments and accelerates virtual screening [23]. In this task, we use the dataset curated from PDBbind [59, 37] and experiment settings in Somnath et al. [49]. We adopt dataset split with 30% and 60% sequence identity thresholds to verify the generalization ability of our models for unseen proteins.

Comparison results are summarized in Table 2, where the baseline results are taken from Somnath et al. [49] and Townshend et al. [56]. Results are reported for 3 experimental runs. The detailed standard deviation of experiment results are provided in Appendix G. Note that we include the results from Atom3D [56] for complete comparison with previous methods. However, the models in Atom3D [56] are trained with binding pockets only, making the task less challenging, while other methods do not consider such prior information in the input. The results show that our methods achieve either best or second best results on both splits and obtain significantly better results than

Table 2: Results on protein-ligand binding affinity prediction task. The top two results for each metric are highlighted as **1st** and **2nd**. \* denotes methods trained with the complex binding pockets only.

Method	Sequence Identity 30%			Sequence Identity 60%		
	RMSE	Pearson	Spearman	RMSE	Pearson	Spearman
DeepDTA [43]	1.866	0.472	0.471	1.762	0.666	0.663
Bepler and Berger (2019) [3]	1.985	0.165	0.152	1.891	0.249	0.275
TAPE [46]	1.890	0.338	0.286	1.633	0.568	0.571
ProtTrans [11]	1.544	0.438	0.434	1.641	0.595	0.588
MaSIF [14]	1.484	0.467	0.455	1.426	0.709	0.701
Atom3D-3DCNN* [56]	<b>1.416</b>	<u>0.550</u>	<b>0.553</b>	1.621	0.608	0.615
Atom3D-ENN* [56]	1.568	0.389	0.408	1.620	0.623	0.633
Atom3D-GNN* [56]	1.601	0.545	0.533	1.408	0.743	0.743
IEConv [21]	1.554	0.414	0.428	1.473	0.667	0.675
Holoprot-Full Surface [49]	1.464	0.509	0.500	1.365	0.749	0.742
Holoprot-Superpixel [49]	1.491	0.491	0.482	1.416	0.724	0.715
ProNet-Amino Acid	<u>1.455</u>	0.536	0.526	1.397	0.741	0.734
ProNet-Backbone	1.458	0.546	0.550	<u>1.349</u>	<u>0.764</u>	<u>0.759</u>
ProNet-All-Atom	1.463	<b>0.551</b>	<u>0.551</u>	<b>1.343</b>	<b>0.765</b>	<b>0.761</b>

previous state-of-the-art methods on the sequence identity 60% split. For our methods at different levels, the all-atom one is best on 5 out of 6 metrics. As the binding affinity may correlate to the chemical reactions on the side chain of a protein, the results may imply that the all-atom method can capture more information for both inter- and intra- protein interaction.

#### 6.4 Protein Protein Interaction

Protein-protein interactions (PPI) are involved in most cellular processes and essential for biological applications [15]. For example, antibody proteins bind to antigens to recognize diseases [56]. Following the dataset [55, 58] and experiment settings in Townshend et al. [56], we predict whether two amino acids contact when the two proteins bind. The evaluation metric is AUROC. Results in Table 3 show that our all-atom level method outperforms all previous methods, improving the result from 0.866 to 0.871. In addition, the results for levels may imply that our all-atom representation can capture more minutiae from side chains on both interacting proteins and thus benefits the binding site prediction.

Table 3: Comparison between existing methods and our methods. The top two results are highlighted as **1st** and **2nd**.

Method	AUROC
Atom3D-3DCNN [56]	0.844
Atom3D-3DGNN [56]	0.669
GVP-GNN [25]	<u>0.866</u>
ProNet-Amino Acid	0.857
ProNet-Backbone	0.858
ProNet-All-Atom	<b>0.871</b>

#### 6.5 Observations and Ablation Studies

**Observations on methods of different levels.** Here, we further study how methods of different levels benefit various downstream tasks. As shown in Table 1, our ProNet-backbone outperforms the methods of the other two levels on function prediction tasks, including fold and reaction classification tasks. This indicates the backbone-level method can capture more details from the folding structure of proteins, making better predictions of protein functions. In contrast to function prediction tasks, as shown in Table 2 and Table 3, our ProNet-all-atom outperforms the methods of the other levels on most metrics of interaction prediction tasks, namely LBA and PPI tasks. This observation implies that our all-atom level method is able to capture fine-grained side chain structure information, eventually contributing to the predictions of binding affinity and binding sites for interacting proteins.

**Ablation studies on all-atom level.** We investigate three ways to achieve complete representations of proteins at all-atom level and explain why we choose the current all-atom level method as proposed in Sec. 2.5. The experiments are conducted on the fold classification dataset. Note that the training time in Table 4 is the average time per epoch, and the three methods use similar epochs to converge. The first baseline is "w/o Hierarchies",

Table 4: Comparison of three all-atom methods on the fold data. The **best** results are highlighted in the table. All the models are trained using the same computing infrastructure (Nvidia GeForce RTX 2080 TI 11GB) for fair comparison.

Method	Time (sec.)		Accuracy (%)			
	Train	Inference	Fold	Sup.	Fam.	Avg.
w/o Hierarchies	181.2	18.1	36.9	49.5	94.2	60.2
Mainstream Hierarchical	148.7	17.7	51.5	68.7	<b>99.0</b>	73.1
ProNet-All-Atom	<b>32.1</b>	<b>6.3</b>	<b>52.1</b>	<b>69.0</b>	<b>99.0</b>	<b>73.4</b>

which denotes that each atom is treated as a node in a 3D protein graph while the graph representation is generated using the complete base model. The performance of this method is unsatisfying, possibly due to the lack of hierarchical information in modeling amino acids. Besides, this method takes a longer time for both training and inference. The second baseline is "Mainstream Hierarchical" as introduced in Sec. 2.2, where we adopt a two-level architecture. The first level follows the "w/o Hierarchies" method, and the second level treats each amino acid as a node with features obtained by aggregating representations of atoms in the corresponding amino acid. The computational cost is high since two models are involved in this method. The third method is "ProNet-All-Atom" as illustrated in Sec. 2.5. As shown in Table 4, this "ProNet-All-Atom" method achieves the best performance among the three methods with less computing time. Considering the efficiency and effectiveness, we choose the last one as our method at all-atom level.

## 7 Conclusion

Protein structures are crucial for protein functions and can be represented at different levels, including the amino acid, backbone, and all-atom levels. We propose ProNet to capture hierarchical relations among different levels and learn protein representations. Particularly, ProNet is complete at all levels, leading to informative and discriminative representations. Results show that ProNet outperforms previous methods on most datasets, and different tasks may require representations at different levels.

## Acknowledgements

This work was supported in part by National Science Foundation grant IIS-2006861 and National Institutes of Health grant U01AG070112.

## References

- [1] Minkyung Baek, Frank DiMaio, Ivan Anishchenko, Justas Dauparas, Sergey Ovchinnikov, Gyu Rie Lee, Jue Wang, Qian Cong, Lisa N Kinch, R Dustin Schaeffer, et al. Accurate prediction of protein structures and interactions using a three-track neural network. *Science*, 373(6557):871–876, 2021.
- [2] Federico Baldassarre, David Menéndez Hurtado, Arne Elofsson, and Hossein Azizpour. GraphQA: protein model quality assessment using graph convolutional networks. *Bioinformatics*, 37(3):360–366, 2021.
- [3] Tristan Bepler and Bonnie Berger. Learning protein sequence embeddings using information from structure. In *International Conference on Learning Representations*, 2019. URL <https://openreview.net/forum?id=SygLehCqtm>.
- [4] Karel Berka, Roman Laskowski, Kevin E Riley, Pavel Hobza, and Jiri Vondrasek. Representative amino acid side chain interactions in proteins. a comparison of highly accurate correlated ab initio quantum chemical and empirical potential procedures. *Journal of Chemical Theory and Computation*, 5(4):982–992, 2009.
- [5] Helen M Berman, John Westbrook, Zukang Feng, Gary Gilliland, Talapady N Bhat, Helge Weissig, Ilya N Shindyalov, and Philip E Bourne. The protein data bank. *Nucleic acids research*, 28(1):235–242, 2000.
- [6] Maxwell L Bileschi, David Belanger, Drew H Bryant, Theo Sanderson, Brandon Carter, D Sculley, Alex Bateman, Mark A DePristo, and Lucy J Colwell. Using deep learning to annotate the protein universe. *Nature Biotechnology*, pages 1–6, 2022.
- [7] Yue Cao, Payel Das, Vijil Chenthamarakshan, Pin-Yu Chen, Igor Melnyk, and Yang Shen. Fold2Seq: A joint sequence (1D)-fold (3D) embedding-based generative model for protein design. In *International Conference on Machine Learning*, pages 1261–1271. PMLR, 2021.
- [8] Bowen Dai and Chris Bailey-Kellogg. Protein interaction interface region prediction by geometric deep learning. *Bioinformatics*, 37(17):2580–2588, 03 2021. ISSN 1367-4803. doi: 10.1093/bioinformatics/btab154. URL <https://doi.org/10.1093/bioinformatics/btab154>.

- [9] Jose M Dana, Aleksandras Gutmanas, Nidhi Tyagi, Guoying Qi, Claire O’Donovan, Maria Martin, and Sameer Velankar. SIFTS: updated structure integration with function, taxonomy and sequences resource allows 40-fold increase in coverage of structure-based annotations for proteins. *Nucleic acids research*, 47(D1):D482–D489, 2019.
- [10] Georgy Derevyanko, Sergei Grudinin, Yoshua Bengio, and Guillaume Lamoureux. Deep convolutional networks for quality assessment of protein folds. *Bioinformatics*, 34(23):4046–4053, 2018.
- [11] Ahmed Elnaggar, Michael Heinzinger, Christian Dallago, Ghalia Rehawi, Yu Wang, Llion Jones, Tom Gibbs, Tamas Feher, Christoph Angerer, Martin Steinegger, et al. Prottrans: Towards cracking the language of life’s code through self-supervised deep learning and high performance computing. *IEEE Transactions on Pattern Analysis and Machine Intelligence*, 2021.
- [12] Matthias Fey and Jan E. Lenssen. Fast graph representation learning with PyTorch Geometric. In *ICLR Workshop on Representation Learning on Graphs and Manifolds*, 2019.
- [13] Alex Fout, Jonathon Byrd, Basir Shariat, and Asa Ben-Hur. Protein interface prediction using graph convolutional networks. *Advances in neural information processing systems*, 30, 2017.
- [14] Pablo Gainza, Freyr Sverrisson, Frederico Monti, Emanuele Rodola, D Boscaini, MM Bronstein, and BE Correia. Deciphering interaction fingerprints from protein molecular surfaces using geometric deep learning. *Nature Methods*, 17(2):184–192, 2020.
- [15] Octavian-Eugen Ganea, Xinyuan Huang, Charlotte Bunne, Yatao Bian, Regina Barzilay, Tommi S. Jaakkola, and Andreas Krause. Independent SE(3)-equivariant models for end-to-end rigid protein docking. In *International Conference on Learning Representations*, 2022. URL <https://openreview.net/forum?id=GQjaI9mLet>.
- [16] Hongyang Gao and Shuiwang Ji. Graph U-nets. In *international conference on machine learning*, pages 2083–2092. PMLR, 2019.
- [17] Hongyang Gao, Yi Liu, and Shuiwang Ji. Topology-aware graph pooling networks. *IEEE Transactions on Pattern Analysis and Machine Intelligence*, 43(12):4512–4518, 2021.
- [18] Justin Gilmer, Samuel S Schoenholz, Patrick F Riley, Oriol Vinyals, and George E Dahl. Neural message passing for quantum chemistry. In *Proceedings of the 34th International Conference on Machine Learning-Volume 70*, pages 1263–1272. JMLR. org, 2017.
- [19] Vladimir Gligorijević, P Douglas Renfrew, Tomasz Kosciolk, Julia Koehler Leman, Daniel Berenberg, Tommi Vatanen, Chris Chandler, Bryn C Taylor, Ian M Fisk, Hera Vlamakis, et al. Structure-based protein function prediction using graph convolutional networks. *Nature communications*, 12(1):1–14, 2021.
- [20] Pedro Hermosilla and Timo Ropinski. Contrastive representation learning for 3D protein structures, 2022. URL [https://openreview.net/forum?id=VINWzIM6\\_6](https://openreview.net/forum?id=VINWzIM6_6).
- [21] Pedro Hermosilla, Marco Schäfer, Matej Lang, Gloria Fackelmann, Pere-Pau Vázquez, Barbora Kozlikova, Michael Krone, Tobias Ritschel, and Timo Ropinski. Intrinsic-extrinsic convolution and pooling for learning on 3D protein structures. In *International Conference on Learning Representations*, 2021. URL <https://openreview.net/forum?id=10mSUR0pwY>.
- [22] Jie Hou, Badri Adhikari, and Jianlin Cheng. DeepSF: deep convolutional neural network for mapping protein sequences to folds. *Bioinformatics*, 34(8):1295–1303, 2018.
- [23] Kexin Huang, Tianfan Fu, Wenhao Gao, Yue Zhao, Yusuf Roohani, Jure Leskovec, Connor Coley, Cao Xiao, Jimeng Sun, and Marinka Zitnik. Therapeutics data commons: Machine learning datasets and tasks for drug discovery and development. *Advances in neural information processing systems*, 2021.
- [24] John Ingraham, Vikas Garg, Regina Barzilay, and Tommi Jaakkola. Generative models for graph-based protein design. *Advances in Neural Information Processing Systems*, 32, 2019.

- [25] Bowen Jing, Stephan Eismann, Pratham N Soni, and Ron O Dror. Equivariant graph neural networks for 3D macromolecular structure. In *The ICML Workshop on Computational Biology*, 2021.
- [26] Bowen Jing, Stephan Eismann, Patricia Suriana, Raphael John Lamarre Townshend, and Ron Dror. Learning from protein structure with geometric vector perceptrons. In *International Conference on Learning Representations*, 2021. URL <https://openreview.net/forum?id=1YLJDvSx6J4>.
- [27] John Jumper, Richard Evans, Alexander Pritzel, Tim Green, Michael Figurnov, Olaf Ronneberger, Kathryn Tunyasuvunakool, Russ Bates, Augustin Žídek, Anna Potapenko, et al. Highly accurate protein structure prediction with AlphaFold. *Nature*, 596(7873):583–589, 2021.
- [28] Diederik P Kingma and Jimmy Ba. Adam: A method for stochastic optimization. *International Conference on Learning Representation*, 2014.
- [29] Thomas N Kipf and Max Welling. Semi-supervised classification with graph convolutional networks. In *International Conference on Learning Representations*, 2017.
- [30] Johannes Klicpera, Janek Groß, and Stephan Günnemann. Directional message passing for molecular graphs. In *International Conference on Learning Representations (ICLR)*, 2020.
- [31] Johannes Klicpera, Florian Becker, and Stephan Günnemann. Gemnet: Universal directional graph neural networks for molecules. In A. Beygelzimer, Y. Dauphin, P. Liang, and J. Wortman Vaughan, editors, *Advances in Neural Information Processing Systems*, 2021. URL [https://openreview.net/forum?id=HS\\_s0axS9K-](https://openreview.net/forum?id=HS_s0axS9K-).
- [32] Michael Levitt and Cyrus Chothia. Structural patterns in globular proteins. *Nature*, 261(5561):552–558, 1976.
- [33] Jiahua Li, Shitong Luo, Congyue Deng, Chaoran Cheng, Jiaqi Guan, Leonidas Guibas, Jian Peng, and Jianzhu Ma. Directed weight neural networks for protein structure representation learning. *arXiv preprint arXiv:2201.13299*, 2022.
- [34] Meng Liu, Youzhi Luo, Limei Wang, Yaochen Xie, Hao Yuan, Shurui Gui, Haiyang Yu, Zhao Xu, Jingtun Zhang, Yi Liu, et al. DIG: a turnkey library for diving into graph deep learning research. *Journal of Machine Learning Research*, 22(240):1–9, 2021.
- [35] Yi Liu, Hao Yuan, Lei Cai, and Shuiwang Ji. Deep learning of high-order interactions for protein interface prediction. In *Proceedings of the 26th ACM SIGKDD International Conference on Knowledge Discovery & Data Mining*, pages 679–687, 2020.
- [36] Yi Liu, Limei Wang, Meng Liu, Yuchao Lin, Xuan Zhang, Bora Oztekin, and Shuiwang Ji. Spherical message passing for 3D molecular graphs. In *International Conference on Learning Representations*, 2022. URL <https://openreview.net/forum?id=givsRXs0t9r>.
- [37] Zhihai Liu, Yan Li, Li Han, Jie Li, Jie Liu, Zhixiong Zhao, Wei Nie, Yuchen Liu, and Renxiao Wang. PDB-wide collection of binding data: current status of the PDBbind database. *Bioinformatics*, 31(3):405–412, 2015.
- [38] Michael J Lopez and Shamim S Mohiuddin. *Biochemistry, essential amino acids*. 2020.
- [39] Yi Lu and Stephen Freeland. On the evolution of the standard amino-acid alphabet. *Genome biology*, 7(1):1–6, 2006.
- [40] Alex Morehead, Chen Chen, and Jianlin Cheng. Geometric transformers for protein interface contact prediction. In *International Conference on Learning Representations*, 2022. URL <https://openreview.net/forum?id=CS4463zx6Hi>.
- [41] David L Nelson, Albert L Lehninger, and Michael M Cox. *Lehninger principles of biochemistry*. Macmillan, 2008.
- [42] Marina V Omelchenko, Michael Y Galperin, Yuri I Wolf, and Eugene V Koonin. Non-homologous isofunctional enzymes: a systematic analysis of alternative solutions in enzyme evolution. *Biology direct*, 5(1):1–20, 2010.

- [43] Hakime Öztürk, Arzucan Özgür, and Elif Ozkirimli. DeepDTA: deep drug–target binding affinity prediction. *Bioinformatics*, 34(17):i821–i829, 2018.
- [44] Clare M O’Connor, Jill U Adams, and Jennifer Fairman. Essentials of cell biology. *Cambridge, MA: NPG Education*, 1:54, 2010.
- [45] Adam Paszke, Sam Gross, Francisco Massa, Adam Lerer, James Bradbury, Gregory Chanan, Trevor Killeen, Zeming Lin, Natalia Gimelshein, Luca Antiga, et al. PyTorch: An imperative style, high-performance deep learning library. *Advances in neural information processing systems*, 32, 2019.
- [46] Roshan Rao, Nicholas Bhattacharya, Neil Thomas, Yan Duan, Peter Chen, John Canny, Pieter Abbeel, and Yun Song. Evaluating protein transfer learning with tape. *Advances in neural information processing systems*, 32, 2019.
- [47] Kristof Schütt, Pieter-Jan Kindermans, Huziel Enoc Saucedo Felix, Stefan Chmiela, Alexandre Tkatchenko, and Klaus-Robert Müller. Schnet: A continuous-filter convolutional neural network for modeling quantum interactions. In *Advances in neural information processing systems*, pages 991–1001, 2017.
- [48] Andrew W Senior, Richard Evans, John Jumper, James Kirkpatrick, Laurent Sifre, Tim Green, Chongli Qin, Augustin Žídek, Alexander WR Nelson, Alex Bridgland, et al. Improved protein structure prediction using potentials from deep learning. *Nature*, 577(7792):706–710, 2020.
- [49] Vignesh Ram Somnath, Charlotte Bunne, and Andreas Krause. Multi-scale representation learning on proteins. In A. Beygelzimer, Y. Dauphin, P. Liang, and J. Wortman Vaughan, editors, *Advances in Neural Information Processing Systems*, 2021. URL [https://openreview.net/forum?id=-xEk43f\\_E06](https://openreview.net/forum?id=-xEk43f_E06).
- [50] Velin Z Spassov, Lisa Yan, and Paul K Flook. The dominant role of side-chain backbone interactions in structural realization of amino acid code. chirotor: A side-chain prediction algorithm based on side-chain backbone interactions. *Protein Science*, 16(3):494–506, 2007.
- [51] Hannes Stärk, Octavian Ganea, Lagnajit Pattanaik, Regina Barzilay, and Tommi Jaakkola. EquiBind: Geometric deep learning for drug binding structure prediction. In *International Conference on Machine Learning*, pages 20503–20521. PMLR, 2022.
- [52] Alexey Strokach, David Becerra, Carles Corbi-Verge, Albert Perez-Riba, and Philip M Kim. Fast and flexible protein design using deep graph neural networks. *Cell systems*, 11(4):402–411, 2020.
- [53] Freyr Sverrisson, Jean Feydy, Bruno E Correia, and Michael M Bronstein. Fast end-to-end learning on protein surfaces. In *Proceedings of the IEEE/CVF Conference on Computer Vision and Pattern Recognition*, pages 15272–15281, 2021.
- [54] Seiji Tanaka and Harold A Scheraga. Medium-and long-range interaction parameters between amino acids for predicting three-dimensional structures of proteins. *Macromolecules*, 9(6): 945–950, 1976.
- [55] Raphael Townshend, Rishi Bedi, Patricia Suriana, and Ron Dror. End-to-end learning on 3D protein structure for interface prediction. *Advances in Neural Information Processing Systems*, 32:15642–15651, 2019.
- [56] Raphael John Lamarre Townshend, Martin Vögele, Patricia Adriana Suriana, Alexander Derry, Alexander Powers, Yianni Laloudakis, Sidhika Balachandar, Bowen Jing, Brandon M. Anderson, Stephan Eismann, Risi Kondor, Russ Altman, and Ron O. Dror. ATOM3D: Tasks on molecules in three dimensions. In *Thirty-fifth Conference on Neural Information Processing Systems Datasets and Benchmarks Track (Round 1)*, 2021. URL <https://openreview.net/forum?id=FkdZLpK1M12>.
- [57] Mihaly Varadi, Stephen Anyango, Mandar Deshpande, Sreenath Nair, Cindy Natassia, Galabina Yordanova, David Yuan, Oana Stroe, Gemma Wood, Agata Laydon, et al. AlphaFold Protein Structure Database: Massively expanding the structural coverage of protein-sequence space with high-accuracy models. *Nucleic acids research*, 50(D1):D439–D444, 2022.

- [58] Thom Vreven, Iain H Moal, Anna Vangone, Brian G Pierce, Panagiotis L Kastiris, Mieczyslaw Torchala, Raphael Chaleil, Brian Jiménez-García, Paul A Bates, Juan Fernandez-Recio, et al. Updates to the integrated protein–protein interaction benchmarks: docking benchmark version 5 and affinity benchmark version 2. *Journal of molecular biology*, 427(19):3031–3041, 2015.
- [59] Renxiao Wang, Xueliang Fang, Yipin Lu, and Shaomeng Wang. The PDBbind database: Collection of binding affinities for protein- ligand complexes with known three-dimensional structures. *Journal of medicinal chemistry*, 47(12):2977–2980, 2004.
- [60] Edwin C Webb. *Enzyme nomenclature 1992 : recommendations of the Nomenclature Committee of the International Union of Biochemistry and Molecular Biology on the nomenclature and classification of enzymes*. Academic Press, 1992.
- [61] Zachary Wu, Kadina E Johnston, Frances H Arnold, and Kevin K Yang. Protein sequence design with deep generative models. *Current opinion in chemical biology*, 65:18–27, 2021.
- [62] Tian Xie and Jeffrey C Grossman. Crystal graph convolutional neural networks for an accurate and interpretable prediction of material properties. *Physical review letters*, 120(14):145301, 2018.
- [63] Kevin K Yang, Zachary Wu, and Frances H Arnold. Machine-learning-guided directed evolution for protein engineering. *Nature methods*, 16(8):687–694, 2019.
- [64] Zuobai Zhang, Minghao Xu, Arian Jamasb, Vijil Chenthamarakshan, Aurelie Lozano, Payel Das, and Jian Tang. Protein representation learning by geometric structure pretraining. *arXiv preprint arXiv:2203.06125*, 2022.

# Learning Protein Representations via Complete 3D Graph Networks

## Appendix

### A Side Chain Torsion Angles

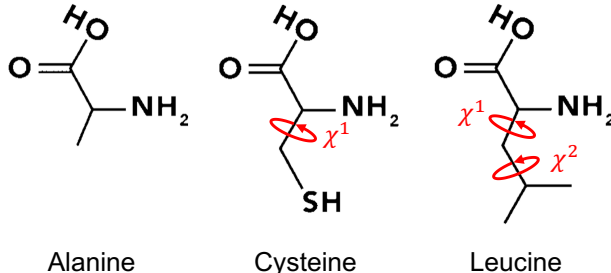


Figure 3: Illustration of amino acid structures. The red circles are side chain torsion angles.

Table 5: Atoms for computing the side chain torsion angles for each amino acid.

	$\chi^1$	$\chi^2$	$\chi^3$	$\chi^4$	$\chi^5$
ALA					
ARG	$N, C_\alpha, C_\beta, C_\gamma$	$C_\alpha, C_\beta, C_\gamma, C_\delta$	$C_\beta, C_\gamma, C_\delta, N_\epsilon$	$C_\gamma, C_\delta, N_\epsilon, C_\zeta$	$C_\delta, N_\epsilon, C_\zeta, N_{\eta 1}$
ASN	$N, C_\alpha, C_\beta, C_\gamma$	$C_\alpha, C_\beta, C_\gamma, O_{\delta 1}$			
ASP	$N, C_\alpha, C_\beta, C_\gamma$	$C_\alpha, C_\beta, C_\gamma, O_{\delta 1}$			
CYS	$N, C_\alpha, C_\beta, S_\gamma$				
GLN	$N, C_\alpha, C_\beta, C_\gamma$	$C_\alpha, C_\beta, C_\gamma, C_\delta$	$C_\beta, C_\gamma, C_\delta, O_{\epsilon 1}$		
GLU	$N, C_\alpha, C_\beta, C_\gamma$	$C_\alpha, C_\beta, C_\gamma, C_\delta$	$C_\beta, C_\gamma, C_\delta, O_{\epsilon 1}$		
GLY					
HIS	$N, C_\alpha, C_\beta, C_\gamma$	$C_\alpha, C_\beta, C_\gamma, N_{\delta 1}$			
ILE	$N, C_\alpha, C_\beta, C_{\gamma 1}$	$C_\alpha, C_\beta, C_{\gamma 1}, C_{\delta 1}$			
LEU	$N, C_\alpha, C_\beta, C_\gamma$	$C_\alpha, C_\beta, C_\gamma, C_{\delta 1}$			
LYS	$N, C_\alpha, C_\beta, C_\gamma$	$C_\alpha, C_\beta, C_\gamma, C_\delta$	$C_\beta, C_\gamma, C_\delta, C_\epsilon$	$C_\gamma, C_\delta, C_\epsilon, N_\zeta$	
MET	$N, C_\alpha, C_\beta, C_\gamma$	$C_\alpha, C_\beta, C_\gamma, S_\delta$	$C_\beta, C_\gamma, S_\delta, C_\epsilon$		
PHE	$N, C_\alpha, C_\beta, C_\gamma$	$C_\alpha, C_\beta, C_\gamma, C_{\delta 1}$			
PRO	$N, C_\alpha, C_\beta, C_\gamma$	$C_\alpha, C_\beta, C_\gamma, C_\delta$			
SER	$N, C_\alpha, C_\beta, O_\gamma$				
THR	$N, C_\alpha, C_\beta, O_{\gamma 1}$				
TRP	$N, C_\alpha, C_\beta, C_\gamma$	$C_\alpha, C_\beta, C_\gamma, C_{\delta 1}$			
TYR	$N, C_\alpha, C_\beta, C_\gamma$	$C_\alpha, C_\beta, C_\gamma, C_{\delta 1}$			
VAL	$N, C_\alpha, C_\beta, C_{\gamma 1}$				

We list atoms used to compute side chain torsion angles for each amino acid in Table 5. Note that AlphaFold2 [27] also considers alternative side chain torsion angles. This is because some side chain parts are 180°-rotation-symmetric, and the torsion angle  $\chi$  and  $\chi + \pi$  result in the same physical structure with the internal atom names changed. But in our method, atom names are given, therefore, we do not need to consider the alternative side chain torsion angles.

### B Proofs

#### B.1 Proof of the Completeness for Backbone Level Representation

*Proof.* Based on Def. 1, we need to prove that the coordinates of all backbone atoms in each amino acid can be uniquely determined given  $\mathcal{F}_{bb}(G)$ . As  $\mathcal{F}(G)_{base}$  is complete for amino acid level, the positions of all alpha carbons in a 3D protein graph are determined as stated in Sec. 3.1. As introduced in Sec.2.4, each backbone triangle is a rigid plane. Then the coordinates of all atoms within each plane can be uniquely determined by the local coordinate system for this backbone plane. Hence, building on the amino acid level, we only need to prove that the local coordinate system for each backbone plane can be uniquely determined.

We prove this by induction. First, we denote  $n$  as the number of nodes, *i.e.*, amino acids, in a 3D protein graph. Apparently, the case  $n = 1$  holds. Assume the case  $n = k$  holds that the GR  $\mathcal{F}(G)_{\text{bb}}$  is complete, thus, the locations of all the  $k$  backbone planes are uniquely determined. Then we need to prove the proposition holds for the  $n = k + 1$  case. Without losing generality, we denote node  $j$  as the  $(k + 1)$ -th node, which is connected to node  $i$  among existing  $k$  nodes, forming a connected graph  $G$  of size  $(k + 1)$ . We then prove that the local coordinate system of the  $(k + 1)$ -th backbone plane is uniquely determined by the proposed Euler angles  $(\tau_{ji}^1, \tau_{ji}^2, \tau_{ji}^3)$ . As illustrated in Fig. 2(b), we use unit vectors  $(\mathbf{x}_i, \mathbf{y}_i, \mathbf{z}_i)$  and  $(\mathbf{x}_j, \mathbf{y}_j, \mathbf{z}_j)$  to denote the backbone coordinate axes of node  $i$  and node  $j$ , respectively. The intersection vector between plane  $\mathbf{x}_i\mathbf{y}_i$  and  $\mathbf{x}_j\mathbf{y}_j$  is denoted as  $\mathbf{n} = \mathbf{z}_i \times \mathbf{z}_j$ . Given the Euler angles  $\tau_{ji}^1, \tau_{ji}^2, \tau_{ji}^3$ , we have

$$\mathbf{x}_i \cdot \mathbf{n} = \cos \tau_{ji}^1, \quad (4)$$

$$\mathbf{x}_i \times \mathbf{n} \cdot \mathbf{z}_i = \sin \tau_{ji}^1, \quad (5)$$

$$\mathbf{z}_i \cdot \mathbf{z}_j = \cos \tau_{ji}^2, \quad (6)$$

$$\mathbf{n} \cdot \mathbf{x}_j = \cos \tau_{ji}^3, \quad (7)$$

$$\mathbf{n} \times \mathbf{x}_j \cdot \mathbf{z}_j = \sin \tau_{ji}^3. \quad (8)$$

Then we sequentially prove by contradiction that vectors  $\mathbf{z}_j$ ,  $\mathbf{x}_j$ , and  $\mathbf{y}_j$  can be uniquely determined by the Euler angles.

Assume the coordination system for the backbone of node  $j$  is not unique, *i.e.*, there are alternative unit vectors  $(\mathbf{x}'_j, \mathbf{y}'_j, \mathbf{z}'_j)$  satisfying Eq. 4- 8. And the alternative intersection vector is denoted as  $\mathbf{n}' = \mathbf{z}_i \times \mathbf{z}'_j$ .

**Step 1:** Prove the intersection  $\mathbf{n}$  is unique.

Substituting  $\mathbf{n}'$  into Eq. 4 and Eq. 5 and subtracting the derived equations with Eq. 4 and Eq. 5, respectively, we can derive that

$$\mathbf{x}_i \cdot (\mathbf{n} - \mathbf{n}') = 0, \quad (9)$$

$$\mathbf{x}_i \times (\mathbf{n} - \mathbf{n}') \cdot \mathbf{z}_i = 0.$$

Since vectors  $\mathbf{x}_i$  and  $(\mathbf{n} - \mathbf{n}')$  are on the same plane perpendicular to  $\mathbf{z}_i$ , there exist  $\lambda \neq 0$  such that

$$\mathbf{x}_i \times (\mathbf{n} - \mathbf{n}') = \lambda \mathbf{z}_i. \quad (10)$$

Then we can derive that

$$\lambda \mathbf{z}_i \cdot \mathbf{z}_i = 0. \quad (11)$$

Since  $\lambda \neq 0$  and  $\mathbf{z}_i$  is a unit vector, Eq. 11 creates a contradiction. Therefore, such  $\mathbf{n}'$  does not exist. The intersection vector  $\mathbf{n}$  of the planes  $\mathbf{x}_i\mathbf{y}_i$  and  $\mathbf{x}_j\mathbf{y}_j$  is uniquely determined by the Euler angle  $\tau_{ji}^1$ .

**Step 2:** Prove  $\mathbf{z}_j$  is unique.

Substituting  $\mathbf{z}'_j$  into Eq. 6 and subtracting the derived equation with Eq. 6, we can derive that

$$\mathbf{z}_i \cdot (\mathbf{z}_j - \mathbf{z}'_j) = 0. \quad (12)$$

Besides, based on the proof in **Step 1**, we have

$$\mathbf{n} = \mathbf{z}_i \times \mathbf{z}_j, \quad (13)$$

$$\mathbf{n} = \mathbf{z}_i \times \mathbf{z}'_j.$$

By subtracting the above equations on both sides, we have

$$\mathbf{z}_i \times (\mathbf{z}_j - \mathbf{z}'_j) = 0. \quad (14)$$

Eq. 12 and Eq. 14 are contradicted since the non-zero vector  $(\mathbf{z}_j - \mathbf{z}'_j)$  is both parallel and perpendicular to the unit vector  $\mathbf{z}_i$ . Thus,  $\mathbf{z}_j$  is uniquely determined by  $\tau_{ji}^1$  and  $\tau_{ji}^2$ .

**Step 3:** Prove  $\mathbf{x}_j$  is unique.

Substituting  $\mathbf{x}'_j$  into Eq. 7 and Eq. 8 and subtracting the derived equations with Eq. 7 and Eq. 8, respectively, we can derive that

$$\mathbf{n} \cdot (\mathbf{x}_j - \mathbf{x}'_j) = 0, \quad (15)$$

$$\mathbf{n} \times (\mathbf{x}_j - \mathbf{x}'_j) \cdot \mathbf{z}_j = 0.$$

As  $(\mathbf{x}_j - \mathbf{x}'_j)$  and  $\mathbf{n}$  are on the same plane perpendicular to  $\mathbf{z}_j$ ,  $\mathbf{n} \times (\mathbf{x}_j - \mathbf{x}'_j) = \mu \mathbf{z}_j$  holds for some  $\mu \neq 0$ . Thus, we can derive that

$$\mu \mathbf{z}_j \cdot \mathbf{z}_j = 0, \quad (16)$$

which is contradicted to the fact that  $\mu \neq 0$  and  $\mathbf{z}_j$  is a unit vector. Therefore,  $\mathbf{x}_j$  can not have alternative solutions, *i.e.*,  $\mathbf{x}_j$  is uniquely determined by  $\tau_{ji}^1, \tau_{ji}^2, \tau_{ji}^3$ .

**Step 4:** Prove  $\mathbf{y}_j$  is unique.

Since  $\mathbf{z}_j$  and  $\mathbf{x}_j$  are unique,  $\mathbf{y}_j = \mathbf{z}_j \times \mathbf{x}_j$  is also uniquely determined by the Euler angles.

The GR  $\mathcal{F}(G)_{\text{bb}} = \mathcal{F}(G)_{\text{base}} \cup \{(\tau_{ji}^1, \tau_{ji}^2, \tau_{ji}^3)\}_{i=1, \dots, n, j \in \mathcal{N}_i}$  on backbone level provides unique representation for different protein backbone structures. Thus, the backbone level representation  $\mathcal{F}(G)_{\text{bb}}$  is complete.  $\square$

With the complete representation, we can compute the unique rotation matrix corresponding to the three static Euler angles  $\tau_{ji}^1, \tau_{ji}^2, \tau_{ji}^3$  as

$$M = M_1 M_2 M_3, \quad (17)$$

where

$$M_1 = \begin{bmatrix} \cos \tau_{ji}^1 & -\sin \tau_{ji}^1 & 0 \\ \sin \tau_{ji}^1 & \cos \tau_{ji}^1 & 0 \\ 0 & 0 & 1 \end{bmatrix}, M_2 = \begin{bmatrix} 1 & 0 & 0 \\ 0 & \cos \tau_{ji}^2 & -\sin \tau_{ji}^2 \\ 0 & \sin \tau_{ji}^2 & \cos \tau_{ji}^2 \end{bmatrix}, M_3 = \begin{bmatrix} \cos \tau_{ji}^3 & -\sin \tau_{ji}^3 & 0 \\ \sin \tau_{ji}^3 & \cos \tau_{ji}^3 & 0 \\ 0 & 0 & 1 \end{bmatrix}.$$

Thus, given the unit vectors  $(\mathbf{x}_i, \mathbf{y}_i, \mathbf{z}_i)$  of node  $i$ , we can derive the backbone coordinate system of node  $j$  as

$$\begin{bmatrix} \mathbf{x}_j \\ \mathbf{y}_j \\ \mathbf{z}_j \end{bmatrix} = M \begin{bmatrix} \mathbf{x}_i \\ \mathbf{y}_i \\ \mathbf{z}_i \end{bmatrix}. \quad (18)$$

## B.2 Proof of the Completeness for All-Atom Level Representation

*Proof.* To prove completeness at the all-atom level, based on Def. 1, we need to prove the positions of all atoms in each amino acid are uniquely determined with  $\mathcal{F}(G)_{\text{all}}$ . Since the GR at the backbone level is complete, the backbone structure of a given protein can be uniquely determined by  $\mathcal{F}(G)_{\text{bb}}$  as introduced in Sec. 3.2. Therefore, for each amino acid  $i$ , we only need to prove that all the atoms of the side chain are uniquely determined by four side chain torsion angles. Note that all bond lengths and bond angles in each amino acid are fully rigid, thus we only consider the unit vector between two atoms in an amino acid. Here we provide rigorous proof for the amino acid cysteine. The proof can be generalized to other types of amino acids.

A cysteine has six atoms, including  $N, C_\alpha, C, O, C_\beta$ , and  $S_\gamma$ . Firstly, the positions of  $N, C_\alpha, C$ , and  $O$  are determined at the backbone level. We can easily further determine the position of  $C_\beta$  since the atoms  $N, C_\alpha, C$ , and  $C_\beta$  are in a rigid group as shown in Table 2 of [27]. Therefore, we only need to prove that the position of atom  $S_\gamma$  is uniquely determined. For an amino acid cysteine with node index  $i$ , we use  $\mathbf{p}_i^1, \mathbf{p}_i^2$ , and  $\mathbf{p}_i^3$  to denote the unit vectors of  $\mathbf{r}_i^{C_\alpha} - \mathbf{r}_i^C, \mathbf{r}_i^{C_\beta} - \mathbf{r}_i^{C_\alpha}$ , and  $\mathbf{r}_i^{S_\gamma} - \mathbf{r}_i^{C_\beta}$ . The unit vectors of  $\mathbf{p}_i^1 \times \mathbf{p}_i^2$  and  $\mathbf{p}_i^2 \times \mathbf{p}_i^3$  are denoted as  $\mathbf{a}_i$  and  $\mathbf{b}_i$ . Given the side chain torsion angle  $\chi_i^1$ , we have

$$\begin{aligned} \mathbf{a}_i \cdot \mathbf{b}_i &= \cos \chi_i^1, \\ \mathbf{a}_i \times \mathbf{b}_i \cdot \mathbf{p}_i^2 &= \sin \chi_i^1. \end{aligned} \quad (19)$$

Assume the position of atom  $S_\gamma$  is not uniquely determined by  $\chi_i^1$ , then there is an alternative position of  $S_\gamma$  satisfying Eq. 19. The new unit vector from  $C_\beta$  to  $S_\gamma$  is denoted as  $\mathbf{p}_i^{3'}$ , and  $\mathbf{b}'_i = \mathbf{p}_i^2 \times \mathbf{p}_i^{3'}$ . Substituting  $\mathbf{b}'_i$  into Eq. 19 and subtracting the derived equations with Eq. 19, we can derive that

$$\begin{aligned} \mathbf{a}_i \cdot (\mathbf{b}_i - \mathbf{b}'_i) &= 0, \\ \mathbf{a}_i \times (\mathbf{b}_i - \mathbf{b}'_i) \cdot \mathbf{p}_i^2 &= 0. \end{aligned} \quad (20)$$

Since vectors  $\mathbf{a}_i$  and  $\mathbf{b}_i - \mathbf{b}'_i$  are perpendicular to  $\mathbf{p}_i^2$ ,  $\mathbf{a}_i \times (\mathbf{b}_i - \mathbf{b}'_i) = \rho \mathbf{p}_i^2$  holds for some  $\rho \neq 0$ . Then we can derive that

$$\mathbf{a}_i \times (\mathbf{b}_i - \mathbf{b}'_i) \cdot \mathbf{p}_i^2 = \rho \mathbf{p}_i^2 \cdot \mathbf{p}_i^2 = 0. \quad (21)$$

Since  $\rho \neq 0$  and  $\mathbf{p}_i^2$  is a unit vector, Eq. 21 creates a contradiction. Therefore, such  $\mathbf{p}_i^{3'}$  does not exist, and the position of atom  $S_\gamma$  is uniquely determined by  $\chi_i^1$ .  $\square$

Table 6: Categorization of existing methods.

Method	Node	Hierarchical Level	Completeness
Ingraham et al. [24]	Amino Acid	Backbone	✗
GVP-GNN [26]	Amino Acid	Backbone	✓
GVP-GNN [25]	Atom	All-Atom	✓
IEConv [21]	Atom	All-Atom	✗
New IEConv [20]	Amino Acid	Backbone	✓
HoloProt [49]	Surface Mesh Vertex/ Amino Acid	Amino Acid + Surface	✗
GearNet [64]	Amino Acid	Amino Acid	✗
GearNet-IEConv [64]	Amino Acid	Backbone	✗
DWNN [33]	Amino Acid	Backbone	✓
<b>Ours</b>	Amino Acid	Amino Acid + Backbone + All-Atom	✓

## C Base Models

### C.1 Geometric Representation

The geometric representation at the amino acid level is  $\mathcal{F}(G)_{\text{base}} = \{(d_{ji}, \theta_{ji}, \phi_{ji}, \tau_{ji})\}_{i=1, \dots, n, j \in \mathcal{N}_i}$  as introduced in Sec. 4. For each edge  $ji$ , we need to compute four geometries based on the positions of nodes  $i, j, i-1, i+1, j-1$  and  $j+1$ . We use  $\mathbf{p}_i^1, \mathbf{p}_i^2, \mathbf{p}_{ij}^1, \mathbf{p}_j^2$  to denote the unit vectors of  $\mathbf{r}_{i-1} - \mathbf{r}_i, \mathbf{r}_{i+1} - \mathbf{r}_i, \mathbf{r}_j - \mathbf{r}_i, \mathbf{r}_{j-1} - \mathbf{r}_j$  and  $\mathbf{r}_{j+1} - \mathbf{r}_j$ . Then the four geometries for edge  $ji$  are computed based on

$$\begin{aligned}
 d_{ji} &= \|\mathbf{p}_{ij}\|_2, \\
 \theta_{ji} &= \arccos(\mathbf{p}_i^1 \cdot \mathbf{p}_{ij}), \\
 \mathbf{n}_1 &= \mathbf{p}_i^1 \times \mathbf{p}_i^2, \quad \mathbf{n}_2 = \mathbf{p}_i^1 \times \mathbf{p}_{ij}, \\
 \phi_{ji} &= \text{atan2}(\mathbf{n}_1 \cdot \mathbf{n}_2, \mathbf{n}_1 \times \mathbf{n}_2), \\
 \mathbf{p}_i &= \begin{cases} \mathbf{p}_i^2, & \text{if } j = i - 1 \\ \mathbf{p}_i^1, & \text{otherwise} \end{cases}, \quad \mathbf{p}_j = \begin{cases} \mathbf{p}_j^2, & \text{if } i = j - 1 \\ \mathbf{p}_j^1, & \text{otherwise} \end{cases}, \\
 \mathbf{n}_3 &= \mathbf{p}_{ij} \times \mathbf{p}_i, \quad \mathbf{n}_4 = \mathbf{p}_{ij} \times \mathbf{p}_j, \\
 \tau_{ji} &= \text{atan2}(\mathbf{n}_3 \cdot \mathbf{n}_4, \mathbf{n}_3 \times \mathbf{n}_4).
 \end{aligned} \tag{22}$$

### C.2 Model Architecture

Similar to SphereNet, our base model architecture contains an embedding layer, several interaction layers, and an output layer. The embedding layer constructs initial node features, edge features, and embeddings of distances and angles in geometric representations. Specifically, we use spherical harmonics to encode distances and angles in geometric representations as shown in Sec. 4 of Liu et al. [36] and Eq. 8-10 of Klicpera et al. [31]. Each of the interaction layers updates node features based on the message passing scheme in Eq. 1. Specifically, for an interaction layer, the inputs are node features, edge features, and basis embeddings of geometric representations, and the outputs are updated node features. Given the inputs, we firstly construct several intermediate updated node features based on the edge features and basis embeddings, separately. Then we perform concatenation of these intermediate updated node features as input to MLPs and thus obtain the final output of this layer. The READOUT function in Eq. 2 is implemented in the output layer. It includes a summation function and several fully-connected layers. Overall, our base model is adapted from the architecture of SphereNet considering our complete and efficient message passing scheme in Eq. 1.

## D Related Work

Based on the analysis in Sec. 2, previous methods on 3D protein graphs can be categorized into three levels, including amino acid level, backbone level, and all-atom level. We summarize existing methods in Table 6. For each method, we provide the component each node represents, the level of information this method incorporates, and the completeness of the method at that level.

Table 7: Model and training hyperparameters for our method on different tasks.

Hyperparameter	Values/Search Space			
	Fold	Reaction	LBA	PPI
Number of layers	3, 4, 5	3, 4, 5	3, 4, 5	3, 4, 5
Hidden dim	64, 128, 256	64, 128, 256	64, 128, 256	64, 128, 256
Cutoff	6, 8, 10	6, 8, 10	6, 8, 10	30
Dropout	0.2, 0.3, 0.5	0.2, 0.3, 0.5	0.2, 0.3	0
Epochs	1000	400	300	20
Batch size	16, 32	16, 32	8, 16, 32, 64	8, 16, 32
Learning rate	1e-4, 2e-4, 5e-4	1e-4, 2e-4, 5e-4	1e-5, 5e-5, 1e-4, 5e-4	1e-4, 2e-4, 5e-4
Learning rate decay factor	0.5	0.5	0.5	0.5
Learning rate decay epochs	100, 150, 200	50, 60, 70, 80	50, 70, 100	4, 8, 10

## E Experimental Setup

This section describes the full experiment setup for each task considered in this paper. All experiments are conducted on a single NVIDIA GeForce RTX 2080 Ti 11GB GPU. The search space for model and training hyperparameters are listed in Table 7. Note that we select hyperparameters at the amino acid, backbone, and all-atom levels by the same search space, and optimal hyperparameters are chosen by the performance on the validation set.

Similar to Hermosilla et al. [21], we apply data augmentation techniques to increase data on fold and reaction classification tasks. Specifically, for the input data, we apply Gaussian noise with a standard deviation of 0.1 and anisotropic scaling in the range [0.9, 1.1] for amino acid coordinates. The same noise is added to the atomic coordinates within the same amino acid, ensuring that the internal structure of each amino acid is not changed. We also mask the amino acid type with a probability of 0.1 or 0.2. For each interaction layer, we employ a Gaussian noise with a standard deviation of 0.025 to both features and Euler angles to further enhance the robustness of our models. We also find that warmup can further improve the performance on reaction classification.

We follow the experiment settings in Somnath et al. [49] for LBA tasks. Since our proposed methods focus on protein representation learning, we employ a two-branch network for a fair comparison. One branch of the network provides the representations for protein structures using our methods and the other branch generates the representations for ligands with a graph convolutional network. We employ the same architecture for the ligand branch as in Somnath et al. [49] and use our models as the protein branch. A few fully-connected layers are then applied to the concatenations of protein and ligand representations to obtain the final representation of the corresponding complex.

## F Dataset Description

**Fold Dataset.** We use the same dataset as in Hou et al. [22] and Hermosilla et al. [21]. In total, this dataset contains 16,292 proteins from 1,195 folds. There are three test sets used to evaluate the generalization ability, namely Fold in which proteins from the same superfamily are unseen during training, Superfamily in which proteins from the same family are unseen during training, and Family in which proteins from the same family are present during training. In this task, 12,312 proteins are used for training, 736 for validation, 718 for Fold, 1,254 for Superfamily, and 1,272 for Family.

**Reaction Dataset.** For reaction classification, the 3D structure for 37,428 proteins representing 384 EC numbers are collected from PDB [5], and EC annotations for each protein are downloaded from the SIFTS database [9]. The dataset is split into 29,215 proteins for training, 2,562 for validation, and 5,651 for testing. Every EC number is represented in all 3 splits, and protein chains with more than 50% similarity are grouped together.

**LBA Dataset.** Following Somnath et al. [49] and Townshend et al. [56], we perform ligand binding affinity predictions on a subset of the commonly-used PDBbind refined set [59, 37]. The curated dataset of 3,507 complexes is split into train/val/test splits based on a 30% or 60% sequence identity threshold to verify the model generalization ability for unseen proteins. For a protein-ligand complex, we predict the negative log-transformed binding affinity  $pK = -\log_{10}(K)$  in Molar units.

**PPI Dataset.** Following the dataset and experiment settings in Townshend et al. [56], we predict whether two amino acids contact when the two proteins bind. We use the Database of Interacting Protein Structures (DIPS) [55] for training and make prediction on the Docking Benchmark 5 (DB5) [58]. The split of protein complexes ensures that no protein in the training dataset has more than 30% sequence identity with any protein in the DIPS test set or the DB5 dataset.

## G Additional Experimental Results

Table 8: Results with standard deviation on LBA dataset split by sequence identity 30%. The top two results for each metric are highlighted as **1st** and **2nd**. \* denotes methods trained with the complex binding pockets only.

Method	Sequence Identity 30%		
	RMSE	Pearson	Spearman
DeepDTA [43]	1.866 ± 0.080	0.472 ± 0.022	0.471 ± 0.024
Bepler and Berger (2019) [3]	1.985 ± 0.006	0.165 ± 0.006	0.152 ± 0.024
TAPE [46]	1.890 ± 0.035	0.338 ± 0.044	0.286 ± 0.124
ProtTrans [11]	1.544 ± 0.015	0.438 ± 0.053	0.434 ± 0.058
MaSIF [14]	1.484 ± 0.018	0.467 ± 0.020	0.455 ± 0.014
Atom3D-3DCNN* [56]	<b>1.416 ± 0.021</b>	<u>0.550 ± 0.021</u>	<b>0.553 ± 0.009</b>
Atom3D-ENN* [56]	1.568 ± 0.012	0.389 ± 0.024	0.408 ± 0.021
Atom3D-GNN* [56]	1.601 ± 0.048	0.545 ± 0.027	0.533 ± 0.033
GVP-GNN* [25]	1.594 ± 0.073	-	-
IEConv [21]	1.554 ± 0.016	0.414 ± 0.053	0.428 ± 0.032
Holoprot-Full Surface [49]	1.464 ± 0.006	0.509 ± 0.002	0.500 ± 0.005
Holoprot-Superpixel [49]	1.491 ± 0.004	0.491 ± 0.014	0.482 ± 0.032
ProNet-Amino Acid	1.455 ± 0.009	0.536 ± 0.012	0.526 ± 0.012
ProNet-Backbone	1.458 ± 0.003	0.546 ± 0.007	0.550 ± 0.008
ProNet-All-Atom	1.463 ± 0.001	<b>0.551 ± 0.005</b>	<u>0.551 ± 0.008</u>

Table 9: Results with standard deviation on LBA dataset split by sequence identity 60%. The top two results for each metric are highlighted as **1st** and **2nd**. \* denotes methods trained with the complex binding pockets only.

Method	Sequence Identity 60%		
	RMSE	Pearson	Spearman
DeepDTA [43]	1.762 ± 0.261	0.666 ± 0.012	0.663 ± 0.015
Bepler and Berger (2019) [3]	1.891 ± 0.004	0.249 ± 0.006	0.275 ± 0.008
TAPE [46]	1.633 ± 0.016	0.568 ± 0.033	0.571 ± 0.021
ProtTrans [11]	1.641 ± 0.016	0.595 ± 0.014	0.588 ± 0.009
MaSIF [14]	1.426 ± 0.017	0.709 ± 0.008	0.701 ± 0.001
Atom3D-3DCNN* [56]	1.621 ± 0.025	0.608 ± 0.020	0.615 ± 0.028
Atom3D-ENN* [56]	1.620 ± 0.049	0.623 ± 0.015	0.633 ± 0.021
Atom3D-GNN* [56]	1.408 ± 0.069	0.743 ± 0.022	0.743 ± 0.027
IEConv [21]	1.473 ± 0.024	0.667 ± 0.011	0.675 ± 0.019
Holoprot-Full Surface [49]	1.365 ± 0.038	0.749 ± 0.014	0.742 ± 0.011
Holoprot-Superpixel [49]	1.416 ± 0.022	0.724 ± 0.011	0.715 ± 0.006
ProNet-Amino Acid	1.397 ± 0.018	0.741 ± 0.008	0.734 ± 0.009
ProNet-Backbone	1.349 ± 0.019	0.764 ± 0.006	0.759 ± 0.001
ProNet-All-Atom	<b>1.343 ± 0.025</b>	<b>0.765 ± 0.009</b>	<b>0.761 ± 0.003</b>